CMS Physics Analysis Summary

Contact: cms-pag-conveners-susy@cern.ch 2016/06/15

Search for new physics in the one soft lepton final state using 2015 data at $\sqrt{s} = 13$ TeV

The CMS Collaboration

Abstract

This note presents the results of a search for new physics using events with one soft lepton and large missing transverse momentum, inclusive in jet flavor and multiplicity. Results are based on a 2.3 fb^{-1} data sample of $\sqrt{s} = 13$ TeV proton-proton collisions collected with the CMS detector. No significant deviations from the standard model expectations are observed, and the results are used to set limits on models featuring compressed spectra. For pair production of top squarks decaying into four bodies, $\widetilde{t} \to b\widetilde{\chi}^0 l(q)\nu(q')$, top squark masses below 340 GeV are excluded for $m_{\widetilde{t}} - m_{\widetilde{\chi}^0} = 50$ GeV. For gluino pair production decaying to $\widetilde{g} \to q\bar{q}\widetilde{\chi}^{\pm}$ followed by $\widetilde{\chi}^{\pm} \to W^*\widetilde{\chi}^0$, with $m_{\widetilde{\chi}^{\pm}} - m_{\widetilde{\chi}^0} = 20$ GeV, gluino masses in the range $900 - 1200$ GeV are excluded for $\widetilde{\chi}^0$ masses in the range $100 - 800$ GeV.

1 Introduction

Searches for new physics based on large transverse momentum imbalance and jets are sensitive to broad classes of models, including supersymmetry (SUSY) [1–8]. Such inclusive all-hadronic searches [9–12] have significant parts of phase space that are limited by irreducible backgrounds from $Z \to \nu\nu$ decays at large Z transverse momentum (p_T). The second largest source of background is typically from boosted Ws with the W decaying to tau plus a neutrino. In many extensions of the standard model (SM), the mass difference between massive particles that interact weakly is generically quite small, giving rise to "compressed spectra". Such small splittings are present even in the SM, with the mass difference between W and Z being barely 10 GeV. When decays between weakly interacting particles of similar masses are allowed, compressed spectra can lead to final states with low p_T (or soft) leptons.

The goal of the present search is to explore the extent to which a generic inclusive soft-lepton analysis can be constructed that reduces these backgrounds significantly, and thus provides sensitivity to weakly interacting massive particle (WIMP) production in cascades or by themselves, when the lowest mass neutral WIMP has a charged partner with a mass within a few to a couple tens of GeV of the neutral WIMP mass. To be orthogonal to existing inclusive single lepton analyses in CMS [13–15], we consider events with one electron or one muon with p_T between 5 and 20 GeV. Depending on the transverse mass between the lepton and missing transverse energy (E_T^{miss}), we find that background suppressions between one and three orders of magnitude can be achieved compared to an all-hadronic analysis [9] in the same kinematic phase space.

This note describes an inclusive search for signatures of new physics containing one soft lepton and large missing transverse momentum, probing a broad range of energies, jet multiplicities and flavors. The search is based on the 2015 dataset collected by the CMS experiment at the LHC: 2.3 fb^{-1} of pp collisions at a center-of-mass energy of 13 TeV. The SM backgrounds are rejected by the lepton and E_T^{miss} requirements: large E_T^{miss} and the presence of a lepton reject Multijet QCD and $Z \to \nu\nu$, events with a leptonic W boson are reduced by requiring that the lepton is soft, and dilepton events (top or diboson) are rejected by vetoing a second lepton. Signals can appear in the tails of the transverse mass of lepton and E_T^{miss} (m_T), as well as in the E_T^{miss} and H_T tails. Jet multiplicity (N_{jets}) and flavor (N_{b-tags}) are used to further classify the search regions.

No significant excesses are found beyond the background predictions in the 2015 data. To demonstrate the sensitivity of the search, we set limits on the production cross-sections for simplified models of third generation squark and gluino pair production as illustrated in Figure 1, as a function of the mass of the produced particles and the lightest super-symmetric particle (LSP). The simplified models of top squark pair production assume the top squark always decays into 4 daughter particles: $\tilde{t} \to b\tilde{\chi}^0 ff'$, with ff' representing $\ell\nu$ or qq' according to W-like branching factions. The top squark models span a range of possible masses between $100 < m_{\tilde{t}} < 600\,\text{GeV}$ with $10 < (m_{\tilde{t}} - m_{\tilde{\chi}^0}) < 80\,\text{GeV}$. The gluino pair-production models assume a 100% branching fraction for $\tilde{g} \to q\bar{q}\tilde{\chi}^{\pm}$. The mass splitting between the chargino and $\tilde{\chi}^0$ in these models is fixed at $\Delta m = 20\,\text{GeV}$, and the chargino always decays to an off-shell W and LSP ($\tilde{\chi}^{\pm} \to ff'\tilde{\chi}^0$), with ff' representing the W^* decay. In this model, the gluino and $\tilde{\chi}^0$ masses are varied between $600 < m_{\tilde{g}} < 1700\,\text{GeV}$ and $0 < m_{\tilde{\chi}^0} < 1150\,\text{GeV}$.

To facilitate application of our search results to a wide range of other models, we provide 95% C.L. limits on signal yields for several well motivated aggregate signal regions, in addition to the main search results.

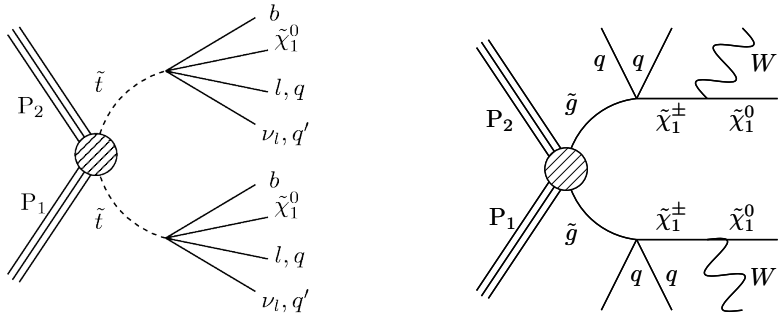

Figure 1: Feynman diagrams illustrating the signal processes considered. The left diagram depicts the 4-body decay of the top squark, $\widetilde{t} \to b\widetilde{\chi}^0 l(q)\nu(q\prime)$. The right diagram depicts gluino pair-production, where the gluinos always decay through a chargino to a W and LSP, $\widetilde{g} \to q\bar{q}\widetilde{\chi}^\pm \to q\bar{q}W\widetilde{\chi}^0$. Both models can decay into final states with 0, 1, or 2 leptons.

2 Monte Carlo simulation

Monte Carlo (MC) simulations are used in the estimate of the SM backgrounds (see Section 5), as well as to estimate the efficiency to select events from different new physics scenarios. The single top, multi-boson and ttV samples are generated with MADGRAPH_aMC@NLO 2.2 [16] or with POWHEG v2 [17, 18], while all other background and control samples, as well as the signal samples of gluino and squark pair production, are generated with the MADGRAPH 5 generator [19]. In the signal samples, off-shell decays are processed by PYTHIA 8.2 [20] in a single three- or four-body step. The decay kinematics is based on phase-space, and does not account for width, life-time, and polarization, which can have large effects as discussed here [21]: this is true for the three-body decay of the chargino ($\widetilde{\chi}^\pm \to ff'\widetilde{\chi}^0$), as well as for the top squark four-body decay ($\widetilde{t} \to b\widetilde{\chi}^0 ff'$). In all cases, the generated events are interfaced with PYTHIA 8.2 for fragmentation and parton showering. The detector simulation is performed using a Geant4-based model [22] of the CMS detector for the SM background samples, and using the CMS fast simulation package [23] for the signal samples. The event reconstruction, described below, is performed in the same way for simulated events and collision data.

3 CMS detector and event reconstruction

The central feature of the CMS apparatus is a superconducting solenoid of 6 m internal diameter, providing a magnetic field of 3.8 T. Within the superconducting solenoid volume are a silicon pixel and strip tracker, a lead tungstate crystal electromagnetic calorimeter (ECAL), and a brass and scintillator hadron calorimeter (HCAL), each composed of a barrel and two endcap sections. Forward calorimeters extend the pseudorapidity [24] coverage provided by the barrel and endcap detectors. Muons are measured in gas-ionization detectors embedded in the steel flux-return yoke outside the solenoid.

Events are processed using the particle-flow (PF) algorithm [25, 26], which reconstructs and identifies each individual particle with an optimized combination of information from the various elements of the CMS detector. The energy of photons is directly obtained from the ECAL measurement, corrected for zero-suppression effects. The energy of electrons is determined from a combination of the electron momentum at the primary interaction vertex as determined by the tracker, the energy of the corresponding ECAL cluster, and the energy sum of all bremsstrahlung photons spatially compatible with originating from the electron track. The energy of muons is obtained from the curvature of the corresponding track. The energy

of charged hadrons is determined from a combination of their momentum measured in the tracker and the matching ECAL and HCAL energy deposits, corrected for zero-suppression effects and for the response function of the calorimeters to hadronic showers. Finally, the energy of neutral hadrons is obtained from the corresponding corrected ECAL and HCAL energy.

For each event, we designate as the primary vertex the one for which the sum p_{T}^2 of the associated particle-flow candidates is largest. Hadronic jets are clustered from neutral particles and charged PF candidates associated to the primary vertex using the anti-k_{T} algorithm [27] with a size parameter R of 0.4. The jet momentum is determined as the vectorial sum of all particle momenta in this jet, and calibrated using the standard set of corrections, similar to the procedure used during the 8 TeV run [28]. Additional selection criteria are applied to each event to remove spurious jet-like features originating from isolated noise patterns in certain HCAL regions. The missing transverse momentum vector $\vec{p}_{\mathrm{T}}^{\,\mathrm{miss}}$ is defined as the projection on the plane perpendicular to the beams of the negative vector sum of the momenta of all reconstructed particles in an event. Its magnitude is referred to as $E_{\mathrm{T}}^{\mathrm{miss}}$. The transverse hadronic energy, H_{T}, is defined as the scalar sum of the jet transverse momenta while the missing transverse hadronic momentum, $\vec{H}_T^{\mathrm{miss}}$, is obtained from the negative vector sum of the momenta of the jets. In this analysis, H_{T}, $\vec{H}_T^{\mathrm{miss}}$ and N_{jets}, the number of jets, are all calculated using jets with $p_{\mathrm{T}} > 30\,\mathrm{GeV}$ and $|\eta| < 2.5$. Jets originating from b-quarks are identified by the combined secondary vertex (CSV) algorithm. We use a working point with a tagging efficiency of approximately 65% for jets originating from b-quarks typical in top pair events and a corresponding mis-tag rate for jets originating from light flavor quarks of about 1.5% [29]. When counting the number of b-jets, $N_{\mathrm{b-tags}}$, we consider jets with $p_{\mathrm{T}} > 20\,\mathrm{GeV}$ and $|\eta| < 2.5$, but we also distinguish between the number of soft ($N_{\mathrm{b-tags}}^{\mathrm{soft}}$, with $20 < p_{\mathrm{T}} < 50\,\mathrm{GeV}$) or hard ($N_{\mathrm{b-tags}}^{\mathrm{hard}}$, with $p_{\mathrm{T}} > 50\,\mathrm{GeV}$) b-jets.

Electrons and muons are identified using two selections: loose and tight. These selections are based on track impact parameter variables and on PF isolation, defined below. In addition, for electrons only, the shape of the energy deposits, the ratio of energy in associated hadron and electromagnetic calorimeter cells (H/E), and the matching between the calorimetric energy deposits and the associated track are also used [30]. Two types of PF isolation are employed, differing in the size of the cone. Both are calculated as a scalar sum of transverse momenta of neutral PF candidates and charged PF candidates associated to the primary vertex, and both are corrected for the effects of pile-up. Standard isolation (I_{03}) is calculated in a cone of $\Delta R = 0.3$, while mini-isolation (I_{mini}) is calculated in a $\Delta R = 0.2(0.05)$ cone for lepton $p_{\mathrm{T}} < 50\,\mathrm{GeV}(> 200\,\mathrm{GeV})$ and $\Delta R = 10\,\mathrm{GeV}/p_{\mathrm{T}}$ for lepton p_{T} in the $[50, 200]\,\mathrm{GeV}$ range. Loose leptons are required to have $I_{\mathrm{mini}} < 0.5 p_{\mathrm{T}}$, while tight leptons are required to have $I_{\mathrm{mini}} < 0.1 p_{\mathrm{T}}$ and $I_{03} < 0.2 p_{\mathrm{T}}$. To avoid counting leptons as jets, the closest jet to a selected lepton (electron or muon) passing the loose requirements is removed from the event, if the jet axis is within $\Delta R < 0.4$ of the lepton. The $m_{\mathrm{T}}(\vec{\ell}, \vec{p}_{\mathrm{T}}^{\,\mathrm{miss}})$ or m_{T}, variable is defined as $\sqrt{2 p_{\mathrm{T}} E_{\mathrm{T}}^{\mathrm{miss}} (1 - \cos\Delta\phi)}$, where p_{T} is the lepton transverse momentum and $\Delta\phi$ is the azimuthal angle between the lepton and the $\vec{p}_{\mathrm{T}}^{\,\mathrm{miss}}$ vector.

Isolated PF charged hadrons associated to the primary vertex, or isolated tracks, are used in a second lepton veto to identify 1-prong hadronic taus and to recover efficiency for electron and muon identification. These tracks are selected based on a track-isolation, $I_{\mathrm{track}} < 0.1/p_{\mathrm{T}}$, which sums transverse momenta of other PF charged hadrons associated to the primary vertex in a cone of $\Delta R = 0.3$ around the isolated track.

4 Event selection

We select events with one tight electron or muon with $5 < p_{\mathrm{T}} < 20\,\mathrm{GeV}$ and with $|\eta| < 1.4442$ for electrons, $|\eta| < 1.479$ for muons. We use an $E_{\mathrm{T}}^{\mathrm{miss}}$ trigger which is fully efficient for $E_{\mathrm{T}}^{\mathrm{miss}} > 200\,\mathrm{GeV}$, so we require the event $E_{\mathrm{T}}^{\mathrm{miss}}$ to be above this value. To ensure that the $E_{\mathrm{T}}^{\mathrm{miss}}$ is dominated by central objects, we use events with $N_{\mathrm{jets}} \geq 1$ and $H_{\mathrm{T}} > 200\,\mathrm{GeV}$, and we require that the magnitude of the vector difference between $\vec{p}_{\mathrm{T}}^{\,\mathrm{miss}}$ and $\vec{H}_T^{\mathrm{miss}}$ is not too large, $(|\vec{p}_{\mathrm{T}}^{\,\mathrm{miss}} - \vec{H}_T^{\mathrm{miss}}|)/E_{\mathrm{T}}^{\mathrm{miss}} < 0.5$. To protect from $E_{\mathrm{T}}^{\mathrm{miss}}$ mismeasurements we define $\Delta\phi_{\mathrm{min}}$ as the minimum difference in azimuthal angle between $\vec{p}_{\mathrm{T}}^{\,\mathrm{miss}}$ and each of the leading four jets with $p_{\mathrm{T}} > 30\,\mathrm{GeV}$ and $|\eta| < 4.7$, and we require $\Delta\phi_{\mathrm{min}} > 0.3$ radians. To reduce the background from dilepton $\mathrm{t\bar{t}}$ events, which can have large values of m_{T}, we reject events if they contain a second electron or muon candidate passing the loose requirements with $p_{\mathrm{T}} > 5\,\mathrm{GeV}$, or an isolated track with $p_{\mathrm{T}} > 10\,\mathrm{GeV}$. We reject events with $m_{\mathrm{T}} < 20\,\mathrm{GeV}$ to reduce $Z \to \tau\tau$ background in which one tau decays hadronically (forming a jet) and one tau decays leptonically resulting in very low m_{T} between the tau decay products (lepton and neutrino).

Following the baseline selection above, we categorize events in different exclusive topological regions according to their visible (H_{T}) and invisible ($E_{\mathrm{T}}^{\mathrm{miss}}$) energy, their multiplicity (N_{jets}) and flavor content ($N_{\mathrm{b-tags}}^{\mathrm{soft}}$, $N_{\mathrm{b-tags}}^{\mathrm{hard}}$). The m_{T} variable is then used to isolate W and single-lepton top events, which typically have $m_{\mathrm{T}} < m_W$.

First we define 3 "tail" topological regions in the main kinematic variables:

- $N_{\mathrm{b-tags}}$ (soft or hard) ≥ 3
- $E_{\mathrm{T}}^{\mathrm{miss}} > 500$ and $N_{\mathrm{b-tags}} \leq 3$
- $H_{\mathrm{T}} > 1000\,\mathrm{GeV}$, $N_{\mathrm{b-tags}} \leq 3$ and $E_{\mathrm{T}}^{\mathrm{miss}} < 500\,\mathrm{GeV}$)

Then we divide the remaining phase space ($N_{\mathrm{b-tags}} \leq 3$, $E_{\mathrm{T}}^{\mathrm{miss}} < 500\,\mathrm{GeV}$, $H_{\mathrm{T}} < 1000\,\mathrm{GeV}$) to create the remaining topological regions:

- $E_{\mathrm{T}}^{\mathrm{miss}}$: [200, 300], [300,500] GeV. These regions are merged in the 1 jet regions with b-tags.
- $N_{\mathrm{b-tags}}$: $N_{\mathrm{b-tags}} = 0$, $N_{\mathrm{b-tags}}^{\mathrm{soft}} = [1,2]$ and $N_{\mathrm{b-tags}}^{\mathrm{hard}} = 0$, $N_{\mathrm{b-tags}}^{\mathrm{hard}} = [1,2]$. They are referred to as '0 b', 'soft b' and 'hard b' regions, respectively.
- N_{jets}: in the 0 b-tag region, the bins are: 1, 2-3, 4-5, ≥ 6 jets. In regions with b-tags the last two bins are merged, giving: 1, 2-3 , ≥ 4 jets.

We further subdivide each topological region in 3 bins of m_{T}: [20, 90], [90, 120], $> 120\,\mathrm{GeV}$, also referred to as low, medium and high m_{T}. This classification results in 21 topological regions, each divided in 3 m_{T} bins for a total of 63 signal regions.

5 Backgrounds

Standard model backgrounds entering the signal regions fall into three categories:

- Single lepton: events with a single leptonically decaying W boson, resulting from W + jets, top ($\mathrm{t\bar{t}}$ or single top), or rare processes, which contain genuine $E_{\mathrm{T}}^{\mathrm{miss}}$ from the W neutrino. This background is greatly reduced by requiring that the lepton has low p_{T}, and by probing the m_{T} distribution at values larger than the W mass. This background is estimated primarily from a control region based on events with 1 high-p_{T} muon and low $E_{\mathrm{T}}^{\mathrm{miss}}$.

- Dilepton: events with two leptonically decaying W bosons, resulting from top ($t\bar{t}$ or Wt) or diboson processes, which can enter the signal region if one of the two leptons is not found. They amount to a smaller background, but they contain E_T^{miss} from 2 neutrinos, so the m_T distribution does not discriminate against them as effectively as against the single lepton backgrounds. This background is estimated primarily from a dilepton control region, similar to the signal region except for the requirement of a second tight electron or muon.
- Fake lepton: events with no prompt leptons (QCD multijet, $Z \to \nu\nu$), or single lepton events where the real lepton is not found, have a small probability to enter the signal region, if one of the jets is reconstructed as a lepton, or if a non–prompt lepton from a heavy flavor decay passes the tight lepton selection. This background is negligible in the bulk of the m_T distribution, but can become relevant at high m_T, where it is estimated using a tight-to-loose ratio method.

The uncertainties on these three backgrounds, described in the sections below, are summarized in Table 1.

Table 1: Ranges of typical values for different sources of systematic uncertainty on the background estimates.

Source	Single lepton [%]	Dilepton [%]
Lepton efficiency	10	5
b tagging efficiency	0–5	0–2
Jet energy scale	10	5–20
W polarization	10–20	–
W/Top composition	1–10	–
Drell-Yan fraction	–	5–10
Top p_T	1–5	–
PDF variations	–	3–5
Renormalization and factorization scales	1–10	1–10
Limited size of MC samples	1–30	1–50
m_T shape ([90, 120], $>$ 120 GeV)	15, 5–30	30, 50
Fake lepton [%]	100	

5.1 Single lepton background

Background events from single-lepton top (including $t\bar{t}$ and single–top) and W + jets can only enter our signal regions through a very asymmetric leptonic W decay, with a low-p_T lepton (e or μ, including those from a leptonic tau decay) and high-p_T neutrino, resulting in large E_T^{miss}. The single high-p_T lepton control region (CR1L) targets these backgrounds by selecting leptonic W decays which have the opposite asymmetry: a high-p_T lepton and low E_T^{miss}. In this control region, the missing energy requirement is applied to the lepton vector ($p_T > 200, 300, 500$ GeV), while the actual E_T^{miss} is required to be low ($E_T^{miss} < 60$ GeV), with an upper bound that is chosen to have a $p_T(W)$ distribution similar to the one in the signal region. The lepton is required to be a tight muon, to avoid fake electrons from QCD multijet events that appear in the low-E_T^{miss} region, and the events in CR1L are selected based on a single muon trigger. After the baseline selection, we compare the expected statistics, composition, and kinematics of CR1L with those expected for the single lepton background in the baseline signal region. The statistics are found to be very close to the signal region statistics, and the composition comparison shows a larger top fraction, 30% as opposed to 20% in the signal region, which results in small differences in the N_{jets} and N_{b-tags} kinematics, and reasonable agreement otherwise.

We use the data in CR1L to estimate the single lepton background yield in signal region bins, with the aid of MC-based transfer factors that account for the differences in yield and kinematics between CR1L and the signal region. Selected events in CR1L are subdivided into topological regions based on H_{T}, N_{jets}, $N_{\mathrm{b-tags}}$, $E_{\mathrm{T}}^{\mathrm{miss}}$ as described in Section 4, where the lepton p_{T} is substituted for the $E_{\mathrm{T}}^{\mathrm{miss}}$. No categorization is made as a function of m_{T}, both to preserve statistics and because the m_{T} shapes of signal and control region are very different, due to the poor angular resolution of $E_{\mathrm{T}}^{\mathrm{miss}}$ in events with low $E_{\mathrm{T}}^{\mathrm{miss}}$ for CR1L. The single lepton background yield in each signal region, $N_{1\ell}^{\mathrm{SR}}$, is then obtained from the corresponding yield in CR1L, N^{CR1L}, via a transfer factor composed of two parts: $R_{\mathrm{MC}}^{\mathrm{SR/CR1L}}$ accounts for the ratio of cross sections between the two asymmetric W boson decays, while $k_{\mathrm{MC}}\left(m_{\mathrm{T}}\right)$ describes the m_{T} shape of single-lepton background events in the signal region. N^{CR1L} is corrected, based on MC, for the small contribution ($\leq$ 5%) of events with fake leptons or with a second real lepton which is not found by the lepton veto. The transfer factors, R and k_{MC}, are obtained from MC and corrected for known differences between data and simulation. The procedure is summarized by the equation below:

$$N_{1\ell}^{\mathrm{SR}}\left(H_{\mathrm{T}}, E_{\mathrm{T}}^{\mathrm{miss}}, N_{\mathrm{jets}}, N_{\mathrm{b-tags}}^{\mathrm{soft}}, N_{\mathrm{b-tags}}^{\mathrm{hard}}, m_{\mathrm{T}}\right) = N^{\mathrm{CR1L}}\left(H_{\mathrm{T}}, E_{\mathrm{T}}^{\mathrm{miss}}, N_{\mathrm{jets}}, N_{\mathrm{b-tags}}^{\mathrm{soft}}, N_{\mathrm{b-tags}}^{\mathrm{hard}}\right) \times \\ \times R_{\mathrm{MC}}^{\mathrm{SR/CR1L}}\left(H_{\mathrm{T}}, E_{\mathrm{T}}^{\mathrm{miss}}, N_{\mathrm{jets}}, N_{\mathrm{b-tags}}^{\mathrm{soft}}, N_{\mathrm{b-tags}}^{\mathrm{hard}}\right) \times k_{\mathrm{MC}}\left(m_{\mathrm{T}}\right). \quad (1)$$

Other than the MC statistical uncertainties and the uncertainties based on the control region yields, there are several effects that can influence the transfer factors R and k_{MC}. The main systematic uncertainty affecting R is the modeling of the W boson polarization, which describes how the W momentum is transferred to the lepton/neutrino pair. The polarization is studied in an inclusive W sample (orthogonal to the signal region) and found to be well described by the MC. The effect of possible mismodelings of the polarization on the transfer factor is studied, based on the procedure established in [13]. Events are reweighted by $w = 1 \pm \alpha(1 - \cos(\theta^*))^2$, where α is taken to be 0.05 for top events and 0.1 for W + jets events, and where θ^* is the angle in the W rest frame between the charged lepton and the W boson direction in the lab frame. For W + jets events this procedure is also tested by reweighting separately the W^+ and W^-events, leading to a smaller uncertainty. The resulting uncertainty in the transfer factors is 10-20%. Several additional uncertainties are taken into account and propagated to $R_{\mathrm{MC}}^{\mathrm{SR/CR1L}}$. The uncertainty on the relative fraction of W + jets and top events leads to a 1-10% effect on the transfer factors, depending on the topological region. The renormalization and factorization scales uncertainties, as well as the uncertainty on the top p_{T}, result in similar (1-10%) variations, and the uncertainties on parton distribution functions (PDFs) are negligible. The experimental uncertainties on lepton efficiency, b-tagging efficiency and jet energy corrections also result in effects between 1 and 10%.

The distribution of the m_{T} variable at values larger than m_{W} for events with one leptonic W is sensitive to several theoretical and experimental effects. The W mass distribution is different in W + jets and top events, since W bosons in top events have a natural mass constraint at the top mass, and since top events are more likely to include additional neutrinos from the larger b-jet multiplicity. The effect of an uncertainty on the fraction of top events in each signal region can be as large as 10-30% in the second and third m_{T} bin. The main reconstruction uncertainty affecting the high m_{T} bins is the uncertainty on the $E_{\mathrm{T}}^{\mathrm{miss}}$ scale and resolution. We study the $E_{\mathrm{T}}^{\mathrm{miss}}$ uncertainties using a γ + jets sample and we find the data to be well described by the MC: the variations introduced based on this study are of the order of 5-20% in the last two m_{T} bins,

with different effects on W and top. These variations are consistent with those expected from propagating the jet energy scale uncertainties to $E_{\mathrm{T}}^{\mathrm{miss}}$, and thus m_{T}. Based on these studies, we assign uncertainties ranging between 5% and 30% on the m_{T} shape, depending on the relative fraction of W and top in each topological region.

5.2 Dilepton background

Background events from dilepton top ($\mathrm{t\bar{t}}$ or Wt) or diboson can only enter the signal region when one lepton is soft and and the other one is not found by the lepton vetoes. The dilepton control region (CR2L) selection is based on the signal region one, except that the veto on a second loose lepton is replaced by a requirement to find a second tight lepton. To reduce the fake lepton contamination, the second lepton is required to have $p_{\mathrm{T}} > 25\,\mathrm{GeV}$. The expected statistics, composition and kinematics of CR2L are comparable with those expected for the dilepton background in the baseline signal region, with the only noticeable difference in kinematics being due to a larger fraction of predicted Drell-Yan events in CR2L (10% as opposed to 5% in the signal region).

The dilepton background estimate is similar to the single-lepton background estimate, but relies on simulation for both the $E_{\mathrm{T}}^{\mathrm{miss}}$ and m_{T} distributions. This choice is motivated by the very small number of dilepton events expected in both CR2L and the signal region. The estimate is summarized by the following equation:

$$N_{2\ell}^{\mathrm{SR}}\left(H_{\mathrm{T}}, E_{\mathrm{T}}^{\mathrm{miss}}, N_{\mathrm{jets}}, N_{\mathrm{b-tags}}^{\mathrm{soft}}, N_{\mathrm{b-tags}}^{\mathrm{hard}}, m_{\mathrm{T}}\right) = N^{\mathrm{CR2L}}\left(H_{\mathrm{T}}, N_{\mathrm{jets}}, N_{\mathrm{b-tags}}^{\mathrm{soft}}, N_{\mathrm{b-tags}}^{\mathrm{hard}}\right) \times \\ \times R_{\mathrm{MC}}^{\mathrm{SR/CR2L}}\left(H_{\mathrm{T}}, N_{\mathrm{jets}}, N_{\mathrm{b-tags}}^{\mathrm{soft}}, N_{\mathrm{b-tags}}^{\mathrm{hard}}\right) \times k_{\mathrm{MC}}\left(E_{\mathrm{T}}^{\mathrm{miss}}, m_{\mathrm{T}}\right). \quad (2)$$

The dilepton background yield in each signal region, $N_{2\ell}^{\mathrm{SR}}$, is obtained from the corresponding yield in CR2L, N^{CR2L} via a transfer factor composed of two parts: $R_{\mathrm{MC}}^{\mathrm{SR/CR2L}}$ accounts for the ratio of cross sections between events where the second lepton is found or lost, while $k_{\mathrm{MC}}\left(E_{\mathrm{T}}^{\mathrm{miss}}, m_{\mathrm{T}}\right)$ describes the $E_{\mathrm{T}}^{\mathrm{miss}}$ and m_{T} distributions of dilepton background events in the signal region. N^{CR2L} is corrected, based on MC, for the small contribution ($\leq 10\%$) of events in which the soft lepton is fake.

Using events with two identified leptons to predict the yield of events with one lost lepton involves several uncertainties. The first uncertainties to consider are related to the lepton acceptance (1-10%, evaluated by varying renormalization and factorization scales, as well as the PDFs), and lepton efficiency (5%, evaluated by varying the corresponding scale factors for e and μ, and the reconstruction efficiency for hadronic taus). An additional uncertainty is related to the Drell-Yan component in CR2L, which is different from that of the signal region, resulting in a 5-10% effect. Furthermore, we consider uncertainties related to b-tagging, which are negligible, and to jet energy corrections, which are 5-20% depending on the regions.

Additional uncertainties are considered for the MC-based m_{T} and $E_{\mathrm{T}}^{\mathrm{miss}}$ distributions, based on the agreement between data and MC in relevant control regions. For m_{T}, the corresponding distribution in CR2L leads to an uncertainty of 30% and 50% on the the second and third m_{T} bin. For $E_{\mathrm{T}}^{\mathrm{miss}}$, the corresponding distribution in a dilepton $\mathrm{t\bar{t}}$ control region, defined as having at least one b-jet and two leptons with $|m_{\ell\ell} - m_Z| > 15\,\mathrm{GeV}$, leads to uncertainties of 10% and 35% for the $300 < E_{\mathrm{T}}^{\mathrm{miss}} < 500\,\mathrm{GeV}$ and the $E_{\mathrm{T}}^{\mathrm{miss}} > 500\,\mathrm{GeV}$ regions, respectively.

5.3 Fake lepton background

Fake lepton backgrounds in the analysis signal regions (where the term "fake" includes non-prompt leptons from heavy flavor decays) can originate from several processes. Genuine QCD multijet background is very small, due to the large $E_{\mathrm{T}}^{\mathrm{miss}}$ requirement applied to the signal region. On the other hand, electroweak processes with neutrinos in their final states are relevant. These include zero-lepton processes such as $\mathrm{Z} \to \nu\nu$, as well as 1-lepton processes, such as $\mathrm{W}+$ jets and top, where the real lepton is lost and a fake one is found.

As a function of m_{T}, the fake lepton background falls more slowly than the single lepton background, since it is not constrained by $m_{\mathrm{T}} < m_{\mathrm{W}}$, but only by the kinematics of lepton p_{T} and $E_{\mathrm{T}}^{\mathrm{miss}}$. So it is negligible with respect to the uncertainties on the other backgrounds at low and medium m_{T}, where we take the fake lepton prediction from MC with a 100% uncertainty. However, it becomes more relevant at large m_{T}, where we estimate it from data.

We use a tight-to-loose ratio or fake rate method, similar to the one used in the same-sign dilepton analysis [31]. In this technique, a loose-not-tight (L!T) control region is constructed by applying all the kinematic requirements of the signal region, except for the soft lepton which is required to pass the loose identification but fail the tight one. The sum of the L!T control region and the signal region is referred to as the application region. After subtracting the expected contribution from prompt leptons failing the tight identification ($N_{\mathrm{prompt}}^{\mathrm{L!T}}$), the L!T sample is weighted using the tight-to-loose ratio (ϵ_{TL}), i.e. the probability that a fake lepton passing the loose identification also passes the tight one. This probability is measured as a function of lepton p_{T} in a QCD multijet control sample (or measurement region) enriched in fake leptons. The equation describing this estimate is therefore:

$$N_{\mathrm{fakes}}^{\mathrm{SR}} = \sum_{p_{\mathrm{T}}} \left(N_{\mathrm{data}}^{\mathrm{L!T}}(p_{\mathrm{T}}) - N_{\mathrm{prompt}}^{\mathrm{L!T}}(p_{\mathrm{T}}) \right) \times \frac{\epsilon_{\mathrm{TL}}(p_{\mathrm{T}})}{1 - \epsilon_{\mathrm{TL}}(p_{\mathrm{T}})} \tag{3}$$

In this analysis, the measurement region is based on a high statistics sample of events recorded using pure H_{T} triggers. Based on simulation, the prompt lepton contamination is found to be small after requiring that $E_{\mathrm{T}}^{\mathrm{miss}} < 50\,\mathrm{GeV}$ and $m_{\mathrm{T}} < 40\,\mathrm{GeV}$, and the tight-to-loose ratio in the measurement region, measured as a function of lepton p_{T}, is found to be compatible to the one in the application region, leading to good closure of the method in MC. The tight-to-loose ratio is measured to be around 0.1, and the expected fake lepton yield in the last m_{T} bin is O(0.1) events. As a result, the measurement is dominated by the low statistics of the L!T region, leading to uncertainties between 50% and 100% on the predicted yield.

6 Results and interpretation

The estimates of standard model single lepton, dilepton and fake lepton background are combined, and the total is compared to the observed data in each signal region in Figure 2 (top), with all uncertainties related to each background added in quadrature. The data are compatible with the prediction. The total background is also estimated through maximum likelihood (ML) fits to the data in the signal regions themselves, using both the background-only and the background+signal hypotheses. Each ML fit takes as inputs the uncertainties of each background, and their full correlation model, and produces a new set of "post-fit" background estimates, shown in Figure 2 (bottom) for the background-only hypothesis. The post-fit results, combined across all regions, are used to constrain models of new physics employing the $\mathrm{CL_s}$ criterion and an asymptotic formulation [32–35].

Table 2: Ranges of typical values for different sources of systematic uncertainty on the signal yields.

Source	Typical values [%]
Integrated luminosity	2.7
Lepton efficiency	10
Jet energy scale	5
b tagging efficiency	0–20
ISR	15–30
Renormalization and factorization scales	5
Limited size of MC samples	1–70

Typical values of the uncertainties on the signal yield are listed in Table 2. The main uncertainties on the signal yields, other than those of the cross-section calculation, are the MC statistical uncertainty and the uncertainty on modeling of initial-state radiation (ISR). The ISR uncertainty is determined by comparing the p_{T} of the $\mathrm{t\bar{t}}$ system in $\mathrm{t\bar{t}}$ events between data and simulation [36], and results in a 15% (30%) effect for $400 < p_{\mathrm{T}} < 600\,\mathrm{GeV}$ ($p_{\mathrm{T}} > 600\,\mathrm{GeV}$). We apply this uncertainty as a function of the p_{T} of the gluino-gluino (or top squark-squark) system, correlated across search bins. The uncertainty on acceptance is evaluated by varying the renormalization and factorization scales by a factor of two, and it is found to be relatively small, similarly to that on the jet energy scale. A constant value of 5%, correlated across search bins, is used for each of these uncertainties, as well as a 10% uncertainty on lepton efficiency and a 2.7% uncertainty on the integrated luminosity [37]. The b-tagging efficiency is varied separately for both light- and heavy-flavor jets, resulting in uncertainties up to 20%. No additional uncertainty for the acceptance effects of PDF variations is applied because their main effect—modifying the ISR spectrum—is already covered by a dedicated uncertainty. The resulting 95% confidence level (CL) exclusion limits are shown in Figure 3, with the observed (expected) top squark limits reaching masses of 340 (330) GeV and the gluino limits reaching masses of 1.2 (1.1) TeV. In Appendix A, results are also presented in terms of a smaller number of aggregated regions, defined as sums of topologically similar signal regions, to facilitate reinterpretations. In Appendix B, the pre-fit background estimates in the sum of all signal regions are compared to data as a function of kinematic distributions.

7 Summary

This note presents the results of a search for new physics using events with one soft lepton and large $E_{\mathrm{T}}^{\mathrm{miss}}$, inclusive in jet flavor and multiplicity. Results are based on a 2.3 fb^{-1} data sample of $\sqrt{s} = 13$ TeV proton-proton collisions collected with the CMS detector. No significant deviations from the standard model expectations are observed, and the results are used to set limits on models featuring compressed spectra. For pair production of top squarks decaying into four bodies, $\widetilde{t} \to b\widetilde{\chi}^0 l(q)\nu(q')$, top squark masses below 340 GeV are excluded for $m_{\widetilde{t}} - m_{\widetilde{\chi}^0} = 50\,\mathrm{GeV}$. For gluino pair production decaying to $\widetilde{g} \to q\bar{q}\widetilde{\chi}^{\pm}$ followed by $\widetilde{\chi}^{\pm} \to W^*\widetilde{\chi}^0$, with $m_{\widetilde{\chi}^{\pm}} - m_{\widetilde{\chi}^0} = 20\,\mathrm{GeV}$, gluino masses in the range 900-1200 GeV are excluded for $\widetilde{\chi}^0$ masses in the range 100-800 GeV.

References

[1] P. Ramond, "Dual theory for free fermions", *Phys. Rev. D* **3** (1971) 2415, doi:10.1103/PhysRevD.3.2415.

[2] Y. A. Golfand and E. P. Likhtman, "Extension of the algebra of Poincaré group generators and violation of P invariance", *JETP Lett.* **13** (1971) 323.

[3] A. Neveu and J. H. Schwarz, "Factorizable dual model of pions", *Nucl. Phys. B* **31** (1971) 86, doi:10.1016/0550-3213(71)90448-2.

[4] D. V. Volkov and V. P. Akulov, "Possible universal neutrino interaction", *JETP Lett.* **16** (1972) 438.

[5] J. Wess and B. Zumino, "A Lagrangian model invariant under supergauge transformations", *Phys. Lett. B* **49** (1974) 52, doi:10.1016/0370-2693(74)90578-4.

[6] J. Wess and B. Zumino, "Supergauge transformations in four dimensions", *Nucl. Phys. B* **70** (1974) 39, doi:10.1016/0550-3213(74)90355-1.

[7] P. Fayet, "Supergauge invariant extension of the Higgs mechanism and a model for the electron and its neutrino", *Nucl. Phys. B* **90** (1975) 104, doi:10.1016/0550-3213(75)90636-7.

[8] H. P. Nilles, "Supersymmetry, supergravity and particle physics", *Phys. Rep.* **110** (1984) 1, doi:10.1016/0370-1573(84)90008-5.

[9] CMS Collaboration, "Search for new physics with the MT2 variable in all-jets final states produced in pp collisions at sqrt(s) = 13 TeV", arXiv:1603.04053.

[10] CMS Collaboration, "Search for supersymmetry in the multijet and missing transverse momentum final state in pp collisions at 13 TeV", (2016). arXiv:1602.06581. Submitted to *Phys. Lett. B*.

[11] ATLAS Collaboration, "Search for new phenomena in final states with large jet multiplicities and missing transverse momentum with ATLAS using $\sqrt{s} = 13$ TeV proton–proton collisions", (2016). arXiv:1602.06194. Submitted to *Phys. Lett. B*.

[12] ATLAS Collaboration, "Search for squarks and gluinos in final states with jets and missing transverse momentum at $\sqrt{s} = 13$ TeV with the ATLAS detector", arXiv:1605.03814.

[13] CMS Collaboration, "Search for supersymmetry in events with one lepton in proton-proton collisions at sqrt(s)=13 TeV with the CMS experiment", CMS Physics Analysis Summary CMS-PAS-SUS-15-006, 2015.

[14] CMS Collaboration, "Search for supersymmetry in pp collisions at sqrt(s)= 13 TeV in the single-lepton final state using the sum of masses of large radius jets", CMS Physics Analysis Summary CMS-PAS-SUS-15-007, 2015.

[15] CMS Collaboration, "Search for direct top squark pair production in the single lepton final state at sqrt(s) = 13 TeV", CMS Physics Analysis Summary CMS-PAS-SUS-16-002, 2016.

[16] J. Alwall et al., "The automated computation of tree-level and next-to-leading order differential cross sections, and their matching to parton shower simulations", *JHEP* **07** (2014) 079, doi:10.1007/JHEP07(2014)079, arXiv:1405.0301.

[17] S. Alioli, P. Nason, C. Oleari, and E. Re, "NLO single-top production matched with shower in POWHEG: s- and t-channel contributions", *JHEP* **09** (2009) 111, doi:10.1088/1126-6708/2009/09/111, arXiv:0907.4076. [Erratum: doi:10.1007/JHEP02(2010)011].

[18] E. Re, "Single-top Wt-channel production matched with parton showers using the POWHEG method", *Eur. Phys. J. C* **71** (2011) 1547, doi:10.1140/epjc/s10052-011-1547-z, arXiv:1009.2450.

[19] J. Alwall et al., "MadGraph 5: going beyond", *JHEP* **06** (2011) 128, doi:10.1007/JHEP06(2011)128, arXiv:1106.0522.

[20] T. Sjostrand, S. Mrenna, and P. Z. Skands, "A Brief Introduction to PYTHIA 8.1", *Comput. Phys. Commun.* **178** (2008) 852–867, doi:10.1016/j.cpc.2008.01.036, arXiv:0710.3820.

[21] R. Grber, M. M. Mhlleitner, E. Popenda, and A. Wlotzka, "Light Stop Decays: Implications for LHC Searches", *Eur. Phys. J.* **C75** (2015) 420, doi:10.1140/epjc/s10052-015-3626-z, arXiv:1408.4662.

[22] GEANT4 Collaboration, "GEANT4—a simulation toolkit", *Nucl. Instrum. Meth. A* **506** (2003) 250, doi:10.1016/S0168-9002(03)01368-8.

[23] S. Abdullin et al., "The fast simulation of the CMS detector at LHC", *J. Phys. Conf. Ser.* **331** (2011) 032049, doi:10.1088/1742-6596/331/3/032049.

[24] CMS Collaboration, "The CMS experiment at the CERN LHC", *JINST* **3** (2008) S08004, doi:10.1088/1748-0221/3/08/S08004.

[25] CMS Collaboration, "Particle-Flow Event Reconstruction in CMS and Performance for Jets, Taus, and MET", Technical Report CMS-PAS-PFT-09-001, CERN, 2009.

[26] CMS Collaboration, "Commissioning of the Particle-flow Event Reconstruction with the first LHC collisions recorded in the CMS detector", Technical Report CMS-PAS-PFT-10-001, CERN, 2010.

[27] M. Cacciari, G. P. Salam, and G. Soyez, "The anti-k_t jet clustering algorithm", *JHEP* **04** (2008) 063, doi:10.1088/1126-6708/2008/04/063, arXiv:0802.1189.

[28] CMS Collaboration, "Determination of jet energy calibration and transverse momentum resolution in CMS", *JINST* **6** (2011) P11002, doi:10.1088/1748-0221/6/11/P11002, arXiv:1107.4277.

[29] CMS Collaboration, "Performance of b-Tagging Algorithms in 50ns Data at 13 TeV", Technical Report CMS-DP-2015-045, Sep, 2015.

[30] CMS Collaboration, "Electron reconstruction and identification at sqrt(s) = 7 TeV", Technical Report CMS-PAS-EGM-10-004, CERN, Geneva, 2010.

[31] CMS Collaboration, "Search for SUSY in same-sign dilepton events at sqrt(s) = 13 TeV", CMS Physics Analysis Summary CMS-PAS-SUS-15-008, 2015.

[32] A. L. Read, "Presentation of search results: The CL_s technique", *J. Phys. G* **28** (2002) 2693, doi:10.1088/0954-3899/28/10/313.

[33] T. Junk, "Confidence level computation for combining searches with small statistics", *Nucl. Instrum. Meth. A* **434** (1999) 435, doi:10.1016/S0168-9002(99)00498-2, arXiv:hep-ex/9902006.

[34] G. Cowan, K. Cranmer, E. Gross, and O. Vitells, "Asymptotic formulae for likelihood-based tests of new physics", *Eur. Phys. J. C* **71** (2011) 1554, doi:10.1140/epjc/s10052-011-1554-0, arXiv:1007.1727.

[35] ATLAS and CMS Collaborations, "Procedure for the LHC Higgs boson search combination in summer 2011", Technical Report ATL-PHYS-PUB-2011-011, CMS-NOTE-2011-005, 2011.

[36] CMS Collaboration, "Search for top-squark pair production in the single-lepton final state in pp collisions at $\sqrt{s} = 8$ TeV", *Eur. Phys. J. C* **73** (2013) 2677, doi:10.1140/epjc/s10052-013-2677-2, arXiv:1308.1586.

[37] CMS Collaboration, "CMS Luminosity Measurement for the 2015 Data Taking Period", CMS Physics Analysis Summary CMS-PAS-LUM-15-001, 2016.

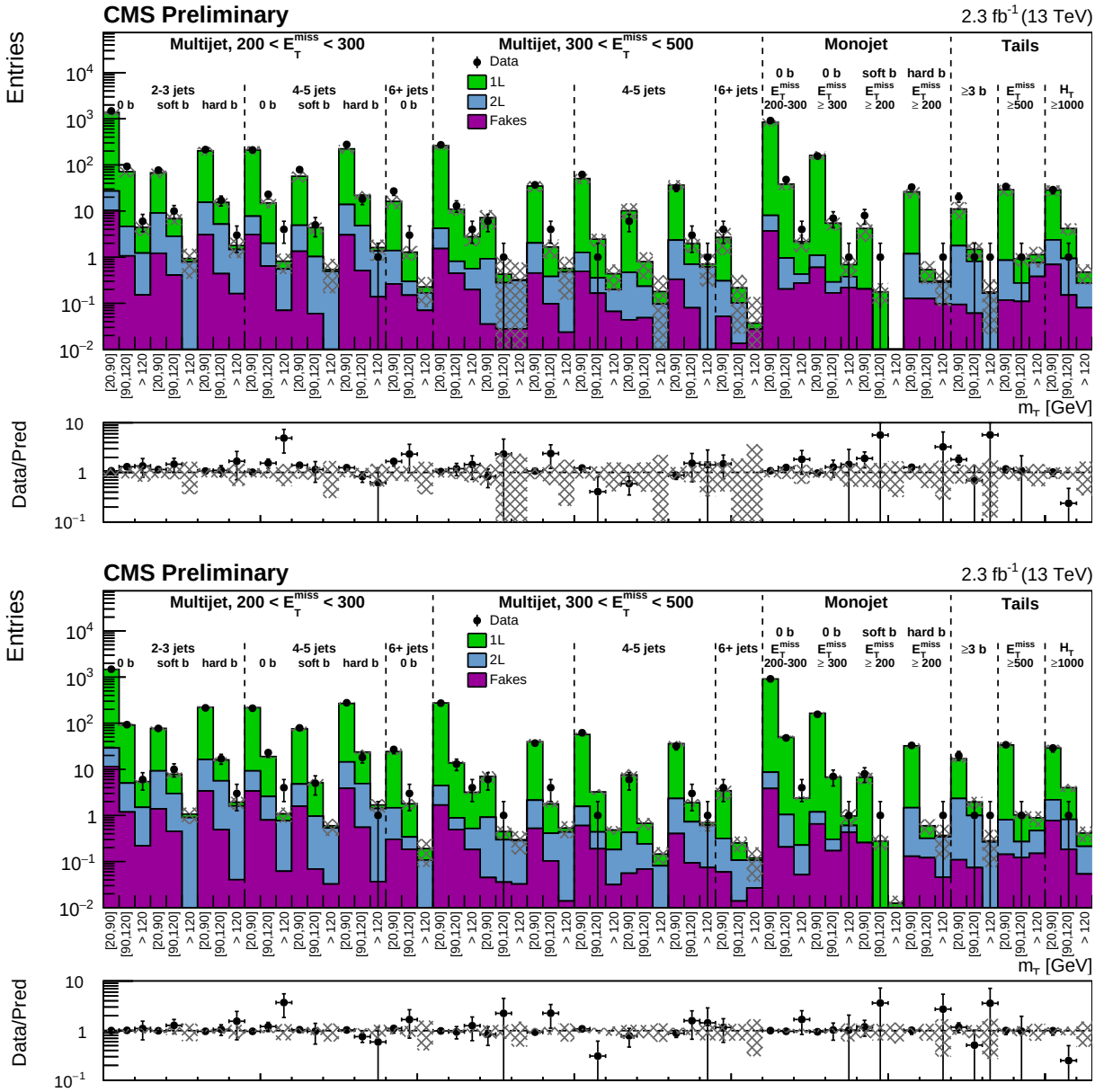

Figure 2: Comparison of estimated background, pre-fit (top) and post-fit (bottom), and observed data events in each signal region. The m_{T} ranges are shown on the x-axis. The grey band in the pre-fit histogram includes the total uncertainty assigned to each background, while in the post-fit histogram it represents the uncertainty measured by the background-only fit.

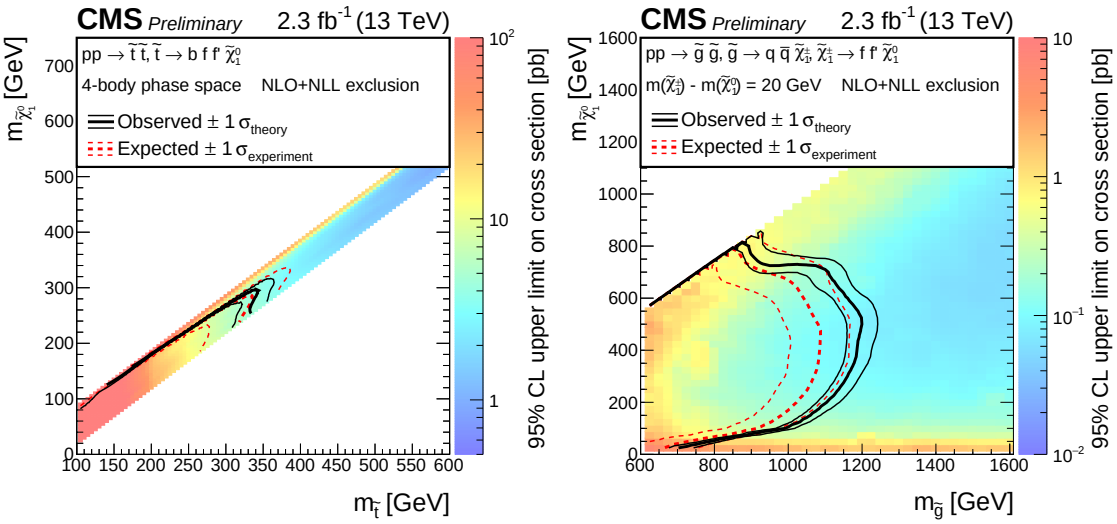

Figure 3: Exclusion limits at 95% CL for top squark (left) and gluino (right) production. The color axis indicates the excluded cross section, while the red and black lines show the expected and observed mass values for which the excluded cross-section is equal to the predicted cross section of the model. The area to the left and below the lines represents the exclusion region.

A Aggregate Signal Regions

This appendix contains the yields and limits for five aggregate signal regions (ASRs), each built by adding several individual signal regions defined in the analysis. Table 3 describes the definitions of the signal regions, and Table 4 (5) gives the predicted post-fit (pre-fit) and observed yields in each region, together with upper limits on the number of signal events. The limits obtained using the ASRs are less stringent than the ones based on the full analysis. This is shown in Table 6, where the upper limit on the cross section for two signal models obtained using the full analysis are compared with the limits obtained using the (post-fit) ASR with the best sensitivity for each model.

Region	H_T[GeV]	E_T^{miss}[GeV]	nJets	nB(soft)	nB(hard)	M_T
0b High M_T	≥ 200	≥ 200	≥ 1	$= 0$	$= 0$	> 120
b-tagged High M_T	≥ 200	≥ 200	≥ 1	nB ≥ 1		> 120
Compressed Top Squark	200–1000	300–500	2–3	1–2	$= 0$	≥ 20
	≥ 200	≥ 200	$= 1$	$= 1$	$= 0$	≥ 20
	≥ 200	≥ 500	≥ 2	≥ 0	≥ 0	≥ 90
	≥ 300	≥ 200	$= 1$	$= 0$	$= 0$	≥ 90
0b ISR	≥ 300	≥ 200	$= 1$	$= 0$	$= 0$	≥ 90
	200–1000	300–500	2–3	$= 0$	$= 0$	≥ 90
	≥ 200	≥ 500	≥ 2	≥ 0	≥ 0	≥ 90
Strong Production	≥ 200	≥ 500	≥ 2	≥ 0	≥ 0	≥ 90
	≥ 1000	200–500	≥ 2	≥ 0	≥ 0	≥ 90

Table 3: Definitions of aggregate signal regions. Each region is obtained by selecting all events that pass the logical OR of the listed selections.

Region	Prediction (Post-Fit)	Observation	N_{95}^{obs}, 15% unc.	N_{95}^{obs}, 30% unc.
0b High M_T	15.1 ± 2.7	19	14	15
b-tagged High M_T	7.6 ± 2.9	7	7	8
Compressed Top Squark	24.4 ± 3.6	25	13	15
0b ISR	26.6 ± 3.2	26	13	14
Strong Production	6.3 ± 1.5	2	4	4

Table 4: Post-fit predictions and observations for the aggregated regions defined in Table 3, together with the observed 95% CL limit on the number of signal events contributing to each region (N_{95}^{obs}). A signal efficiency uncertainty of either 15 or 30% is assumed for calculating the limits.

Region	Prediction (Pre-Fit)	Observation	N_{95}^{obs}, 15% unc.	N_{95}^{obs}, 30% unc.
0b High M_T	13.2 ± 5.4	19	18	19
b-tagged High M_T	7.2 ± 4.6	7	8	9
Compressed Top Squark	20.5 ± 5.6	25	18	20
0b ISR	21.9 ± 6.8	26	19	20
Strong Production	6.7 ± 2.3	2	4	4

Table 5: Pre-fit predictions and observations for the aggregated regions defined in Table 3, together with the observed 95% CL limit on the number of signal events contributing to each region (N_{95}^{obs}). A signal efficiency uncertainty of either 15 or 30% is assumed for calculating the limits.

Signal	Expected limit [pb] (full analysis)	Best ASR	Signal yield (best ASR)	Expected limit [pb] (best ASR)
$pp \to \tilde{t}\tilde{t}$ $\tilde{t} \to b\widetilde{\chi}_1^0 W^*$ $m_{\tilde{t}} = 275$ GeV $m_{\widetilde{\chi}_1^0} = 235$ GeV	8.51	Compressed Top Squark	11	17.02
$pp \to \tilde{g}\tilde{g}$ $\tilde{g} \to qq\widetilde{\chi}_1^{\pm}$,$\widetilde{\chi}_1^{\pm} \to W^*\widetilde{\chi}_1^0$ $m_{\tilde{g}} = 1100$ GeV $m_{\widetilde{\chi}_1^{\pm}} = 620$ GeV $m_{\widetilde{\chi}_1^0} = 600$ GeV	0.21	Strong Production	5	0.23

Table 6: Expected upper limits on the cross section of different simplified models, as determined from the full analysis, are compared to the upper limits obtained using only the aggregate signal region with the best sensitivity to each considered signal model. A 15% uncertainty in the signal selection efficiency is assumed for calculating these limits. The signal yields expected for an integrated luminosity of 2.3 fb are also shown.

B Summary Plots

This appendix contains kinematic distributions for the sum of all signal regions shown in Figure 2. The background distributions are obtained by scaling the MC shape in each individual signal region to the predicted background (pre-fit) in that region, and then summing over all regions. The uncertainties include statistical uncertainties from the control regions yields, as well as systematic uncertainties.

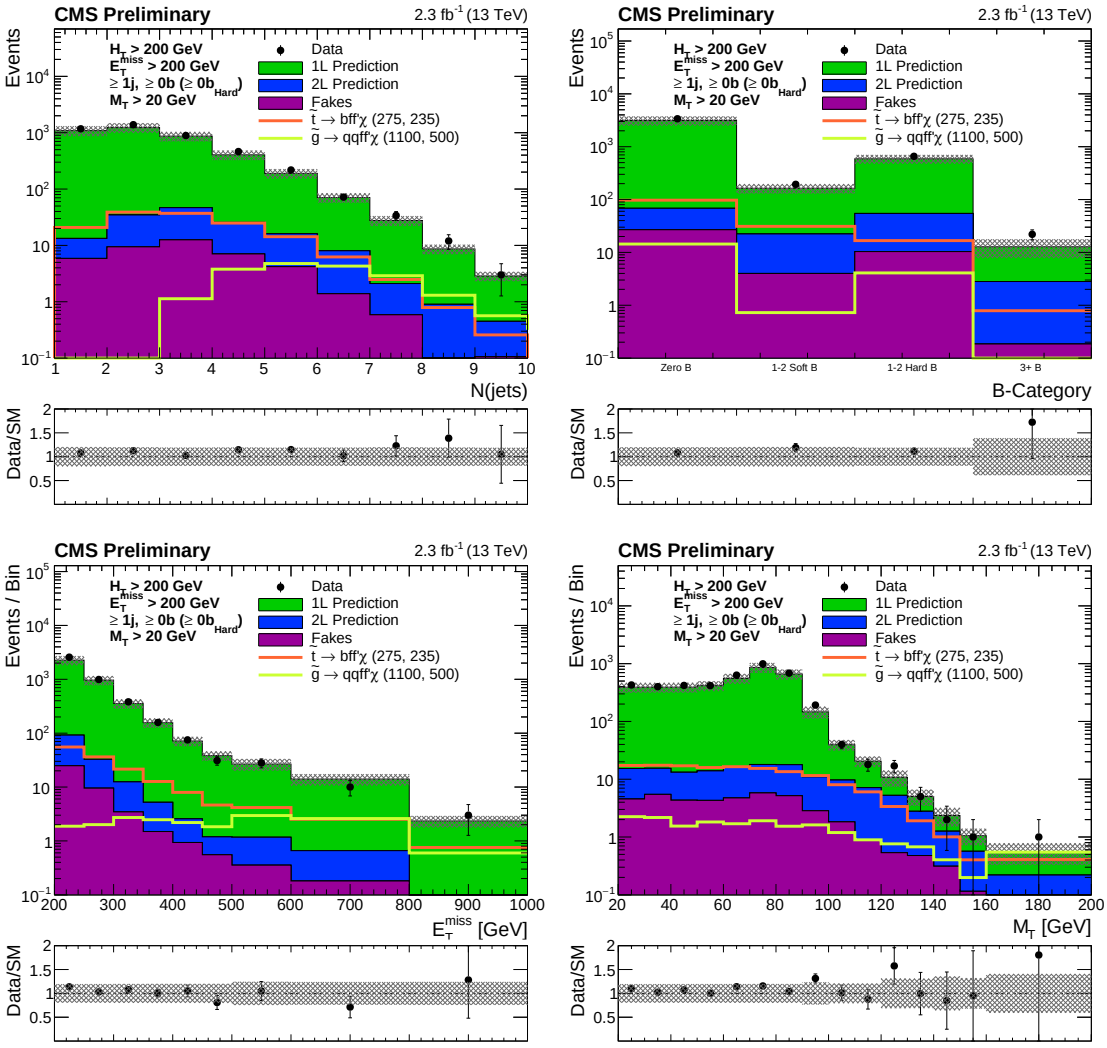

Figure 4: Comparisons of estimated backgrounds and observed data events in the sum of all signal regions, as a function number of jets (top left) heavy flavor category (top right), $E_{\mathrm{T}}^{\mathrm{miss}}$ (bottom left), $m_{\mathrm{T}}(\vec{\ell}, \vec{p}_{\mathrm{T}}^{\,\mathrm{miss}})$ (bottom right). Each estimated background distribution is formed by summing the MC shapes for all signal regions, where each MC shape is first scaled to the predicted background (pre-fit) in that region. The grey band represents the statistical and systematic uncertainty on the estimates.